Stem Cell Research & Therapy

RESEARCH

Open Access

Mesenchymal stromal cells promote the formation of lung cancer organoids via Kindlin-2

Zhilin Sui[1†], Xianxian Wu[1†], Jiaxin Wang[1†], ShihJye Tan[4], Chao Zhao[3], Zhentao Yu[1], Chuanyue Wu[5*], Xiaoxiao Wang[2,4*] and Ling Guo[1,4*]

Abstract

Background Patient-derived lung cancer organoids (PD-LCOs) demonstrate exceptional potential in preclinical testing and serve as a promising model for the multimodal management of lung cancer. However, certain lung cancer cells derived from patients exhibit limited capacity to generate organoids due to inter-tumor or intra-tumor variability. To overcome this limitation, we have created an in vitro system that employs mesenchymal stromal cells (MSCs) or fibroblasts to serve as a supportive scaffold for lung cancer cells that do not form organoids.

Methods We successfully established an MSCs/fibroblast co-culture system to form LCOs. We analyzed the morphological and histological similarities between LCOs co-cultured with fibroblast and primary lung cancer lesions through HE and IF staining. We evaluated whether LCOs co-cultured with fibroblast retained the original genetic mutations of their source tumors based on WES. RNA sequencing was used to analyze the differences in gene expression profiles between LCOs co-cultured with fibroblast and paracancerous organoids (POs). Importantly, we have successfully validated the impact of Kindlin-2 on the regulation of MSCs in organoid formation through lentiviral vector-mediated interference or overexpression of kindlin-2.

Results Our findings demonstrate that the addition of MSCs/fibroblasts to three tumor samples, initially incapable of forming organoids by traditional methods, successfully facilitated the cultivation of tumor organoids. Importantly, these organoids co-cultured with fibroblast faithfully recapitulate the tissue morphology of original lung tumors and replicate the genetic profile observed in the parental tumors even after prolonged in vitro culture. Moreover, drug responses exhibited by these organoids co-cultured with MSCs/fibroblasts are consistent with those observed in the original tumors. Mechanistically, we have also identified kindlin-2 as a crucial regulator linking extracellular matrix (ECM) and mitochondria that influence MSC/fibroblast-mediated support for tumor organoid formation.

†Zhilin Sui, Xianxian Wu and Jiaxin Wang contributed equally to this work.

*Correspondence:
Chuanyue Wu
carywu@pitt.edu
Xiaoxiao Wang
wangxx_2005@126.com
Ling Guo
guoling0423@163.com

Full list of author information is available at the end of the article

Conclusion The results obtained from our research enhance the understanding of the mechanisms implicated in the formation of tumor organoids and aid in creating stronger patient-specific tumor organoid models. This advancement supports the refinement of personalized drug response assessments for use in clinical settings.

Keywords Lung cancer organoids (LCOs), Mesenchymal stromal cells (MSCs), Fibroblast, Kindlin-2, Tumor microenvironment (TME)

Graphical Abstract

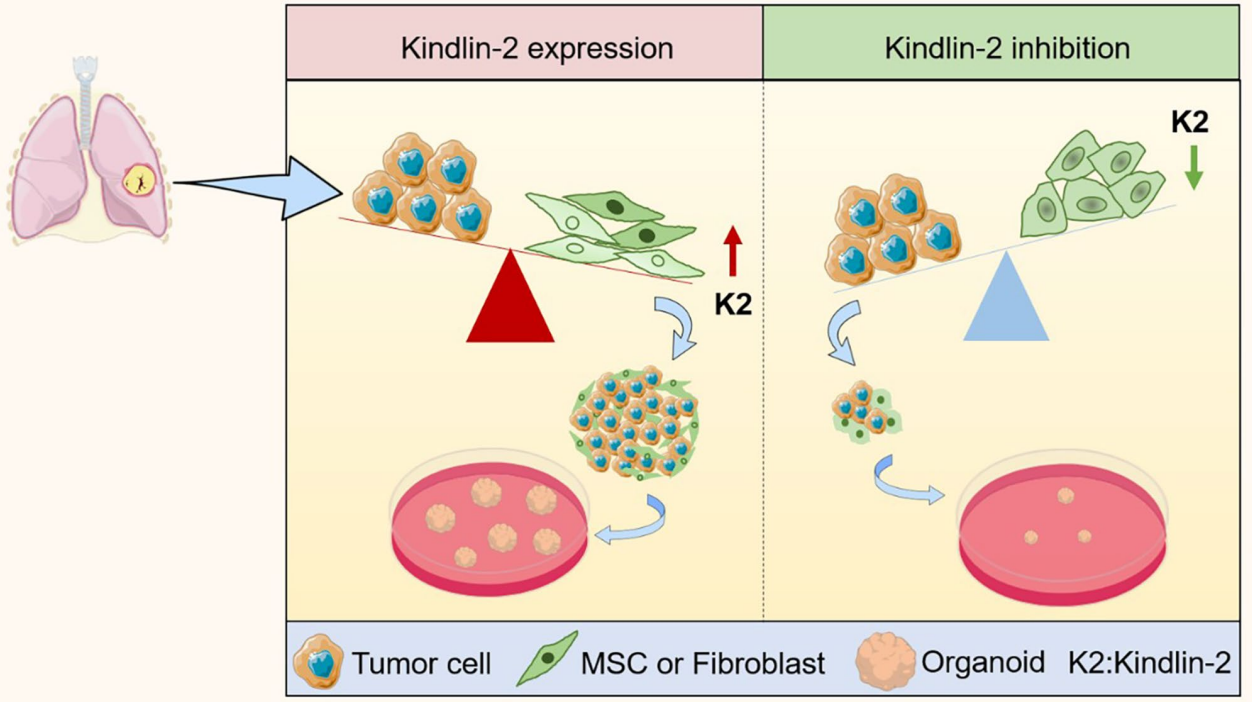

Introduction

Patient-derived lung cancer organoids (PD-LCOs) represent a three-dimensional cultivation of lung cancer cells that are directly propagated from the tissue samples taken from patients with lung cancer. The organoids are cultivated under precise conditions that preserve the histological architecture, genetic variations, and sensitivity to drugs that resemble those found in the original tumor [1–6]. These models derived from patients serve as a system for the rapid screening of prospective treatments, providing scientists with the means to test new drug efficacy and safety in models that closely resemble actual tumors found in vivo [7–10]. Furthermore, PD-LCOs encapsulate the diverse cell populations found in lung cancer, which is crucial for investigating the fundamental mechanisms of disease evolution and the emergence of resistance to treatments [11–13]. By analyzing the genetic and molecular features of organoids derived from patients, researchers can identify biomarkers that predict treatment response or prognosis [14–17]. Patient-derived organoids can incorporate various non-cancerous cell types found within the tumor environment, including MSCs, fibroblasts, and immune cells. This highlights the intricate interplay between cancer cells and their immediate microenvironment [18–20].

A key prerequisite for maintaining primary tumor organoid culture in vitro is a reliable reproduction of the tumor microenvironment (TME) [21], wherein fibroblasts have a crucial function in recapitulating the TME and exerting influence on organoid development [22, 23]. MSCs and fibroblasts share comparable features such as appearance, gene expression patterns, surface antigens, growth, differentiation abilities, and capacity to modulate the immune system, making it challenging to differentiate between them. The profound similarities between these cell types suggest a potential relationship or common lineage [24]. When hMSCs are subjected to a tumor-conditioned medium for an extended duration, they adopt a phenotype resembling that of cancer-associated fibroblasts (CAFs), with myofibroblastic characteristics. Crucially, these cells not only take on the appearance of CAFs but also their functional attributes, demonstrating the capacity to enhance tumor cell proliferation both in laboratory settings and within a live coimplantation

framework. In addition, they display distinctive markers of myofibroblasts such as fibroblast surface protein and α-smooth muscle actin [25]. These observations suggest that MSCs could potentially differentiate into CAFs and could be effectively used to replicate the intricate interplay between tumors and the adjacent stromal tissue. Grasping the function of MSCs within PD-LCOs is crucial for the development of a more accurate representation of lung cancer, which can be utilized for pharmacological evaluations, exploration of tumor biology, and the formulation of tailored treatment strategies.

Kindlin-2, a critical extracellular matrix (ECM) remodeling protein, plays significant biological roles. On one hand, it is involved in integrin-mediated signaling and acts as a bridge between the ECM and intracellular pathways [26–28]; on the other hand, kindlin-2 interacts with PYCR1 to mediate proline biosynthesis-a key process in collagen production and ECM formation [26]. In addition, kindlin-2 is a central player in the activation of lung fibroblasts and the advancement of pulmonary fibrosis [29]. An increased presence of kindlin-2, particularly the FERM domain-containing variant in fibroblasts, has been linked to gastric cancer's epithelial-mesenchymal transition (EMT) and immunosuppressive conditions [30]. Kindlin-2 is necessary to reinforce and develop focal adhesions (FAs) and stress fibers in both activated fibroblasts and myofibroblasts [31]. Additionally, kindlin-2 modulates the survival, differentiation, and migration of mesenchymal stromal [32]. Given these functions, kindlin-2 and its associated signaling pathways are believed to be significant in organoid models.

In this study, we found that 3 patient-derived lung cancer cell samples that failed to form tumor organoids could generate tumor organoids when cultured in vitro with MSCs or paracancerous fibroblasts. When kindlin-2 expression was disrupted in MSCs or paracancerous fibroblasts, tumor organoid formation was significantly reduced in number and size. Overexpression of kindlin-2 in MSCs significantly increased organoid size and organoid number. This implies that the participation of MSCs/fibroblasts could potentially be identified in the development of lung tumor organoids and that kindlin-2 is an important factor regulating the tumor organoid microenvironment. We have established a useful culture technology and platform for tumor organoids, providing a novel experimental method for studying the occurrence and advancement of tumors, TME, and personalized treatment.

Materials and methods

Collection of Tumor samples

Specimens from lung cancer surgeries, ranging in size from 1 to 2.5 cm^3, were swiftly delivered to the research facility following excision. Comprehensive patient clinical data can be found in Supplementary Table S1.

Organoid culture

Fibroblast culture

The fresh tumor sample was washed with cold PBS twice and then minced the tissue into 1–2 mm^3 pieces with scissors. Collected minced tissue into a 15 ml centrifuge tube, added 10 ml collagenase I (3 mg/ml) and a ROCK inhibitor Y-27,632 dihydrochloride (10μM), and then incubated and digested the tissues in a 37 °C cell incubator for 2–3 hours. Filtered the digested tissue using a 70 μM cell strainer to isolate single-cell suspensions from undigested large clusters. Transferred the remaining undigested clusters to a fresh 10 cm cell culture dish containing 10 ml of DMEM, enriched with 10% FBS (Gibco-Invitrogen) and 50 U/mL penicillin/streptomycin (C0222, Beyotime). Moved the cell culture dish into a cell incubator with a 5% CO_2 concentration. After a 5–10 days culture, fibroblasts could be found adhered to the cell culture dish and then refreshed the culture medium. Fibroblasts were passed at a ratio ranging from one to three to one to four every 3–5 days. Then we could collect the fibroblasts with TE buffer for lung cancer cells-fibroblasts co-culture.

Organoid culture with fibroblast/MSCs in Mi-gel

Mi-gel (G23001, Morga) and Mi-gel buffer B (E23001, Morga) were used as the organoids culture matrix material. The Mi-gel was put in a 37 °C incubator for melt, otherwise, the Mi-gel buffer B was put on ice. For the study, the suspension of cells and fibroblasts was acquired from the methods outlined within the "Fibroblast culture". Then the cells were divided into three different groups, lung cancer cells group, lung cancer cells-fibroblasts co-culture group (1:1), and lung cancer cells-MSCs co-culture group (1:1). The cell mixture underwent a PBS wash and was subjected to centrifugation at 1500 rpm for 5 min to eliminate the PBS. This process was repeated twice, followed by an additional centrifugation step aimed at completely removing any remaining liquid. Resuspend cells with melted Mi-gel and Mi-gel buffer B were added, and the ratio of Mi-gel and Mi-gel buffer B was 20:1. The suspension was fully mixed with a pipette, and then dropped the mixture (~ 20 μl per drop) into 6-well cell culture plate, incubated the culture dish in 37 °C cell incubator with 5% CO_2. Once solidified, added 2 ml of lung cancer organoid medium per well, and the medium was refreshed every 3 days. Lung cancer organoid medium was prepared as described in our previously published study [33].

For organoids passaging, we harvested the Mi-gel drops with a cell scalper and smashed the Mi-gel drops into small pieces with 1 ml pipette tips, then collected the

Mi-gel and cell pellet into a 15 ml tube and centrifuged at 1500 rpm for 5 min. Washed the Mi-gel and cell pellet with PBS and then centrifuged at 1500 rpm for 5 min. Removed the PBS and digested the Mi-gel and cell pellet with organoids digestion solution (D23001, Morga) at 37 °C for 5–10 min. Organoids were then centrifuged at 1000 rpm for 5 min. Washed the organoids with culture medium once, and centrifuged again. LCOs were grown for 2–3 weeks and then were passed at a ratio ranging from one to two to one to three.

Ultra-low adsorption culture

The suspension of lung cells and fibroblasts was obtained through the methods described in the "Organoid culture with fibroblast/MSCs in Mi-gel". 1 million lung cancer cells were harvested for the LCCs group and 0.5 million lung cancer cells and 0.5 million fibroblasts were harvested and fully mixed with a 1 ml pipette. Washed the cells with PBS and followed a 1500 rpm centrifugation for 5 min. Removed the PBS and resuspended cells with 10 ml lung cancer organoid medium, then added the cell suspension into a 10 cm ultra-low adsorption cell culture dish. The dish was subsequently positioned within a temperature-controlled cell incubator, maintained at 37 °C, and enriched with a 5% CO_2 environment. The lung cancer organoid medium was refreshed every 3 days. While refreshing the medium, cell suspension was carefully collected and centrifuged to remove the old medium, and added 10 ml fresh medium to the cells.

Hematoxylin and Eosin (HE) staining

To prepare for HE staining, both the organoids were set in 2% agarose, and the fresh tumor samples were fixed using 10% formalin for 24 ~ 48 h. Subsequently, the samples were placed into embedding cassettes and subjected to a dehydration process using an ethanol series: starting with 75% ethanol overnight, followed by 85% ethanol for 3 h, then 95% ethanol for another 3 h, and finally two 1-hour sessions in 100% ethanol. Post-dehydration, the samples in the cassettes were cleared in two 30-minute xylene baths. Afterward, the samples were encased in paraffin. The FFPE specimens, which had been fixed in formalin and embedded in paraffin, were subsequently sectioned into 4 μm-thick slices and subjected to drying at 60 °C for 2 h. After drying, the samples can be effectively cooled to 20 °C and were preserved at 4 °C. The sections were then dewaxed in xylene for three intervals of 10 min each and rehydrated in a descending alcohol series: twice in 100% ethanol, once in 95% ethanol, and once in 70% ethanol, each step lasting 10 min. For HE staining, the slides underwent treatment with hematoxylin, were differentiated, reblued, and counterstained with eosin, and finally sealed using a specific HE staining kit (G11201, Solarbio, Beijing, China).

Immunofluorescence analysis (IF)

For the IF analysis, sections of tissue or LCOs were initially subjected to dewaxing and rehydration. Subsequently, a citrate buffer with a pH of 6.0 was utilized for antigen retrieval. Following that, the sections underwent permeabilization at 20 °C for 30 min using a 0.5% Triton X-100 solution in PBS. Afterward, they underwent blocking by incubating them in a solution consisting of 5% BSA and 0.2% Triton X-100 in PBS for another 30 min at 20 °C. After completing the blocking step, the sections were exposed to appropriate primary antibodies. TTF-1 (A18128, ABclonal), BRG1 (A2117, ABclonal), Cytokeratin 18 (CK18) (A19778, ABclonal), P63 (12143-1-AP, Proteintech), Cytokeratin5/6 (CK5/6) (28506-1-AP, Proteintech), CD56 (A7913, Abclonal), Synaptophysin (syn, A18127, Abclonal), Ki-67 (27309-1-AP, Proteintech), Actin (A12379, Invitrogen), and Integrin β1 (ab24693, Abcam), were utilized for the IF analysis at 4℃ overnight. The slides underwent a PBS wash followed by exposure to diluted secondary antibodies.

DNA extraction and WES (whole-exome sequencing) analysis

Genomic DNA from the tissue samples was extracted using the Tissue Genomic DNA Extraction Kit (DP304-03, Tiangen). The DNA was then fragmented with a Covaris M220 Focused-ultrasonicator (Covaris, Massachusetts), after which sequencing libraries were prepared. The Human Exome 2.0 Plus capture kit (Twist Bioscience) was utilized for exome capture according to the instructions provided by the manufacturer. Sequencing of the final library preparations was carried out on the Illumina NovaSeq 6000 Sequencing System (Illumina), generating 150 bp paired-end reads, at LC-Bio Technology Co., Ltd.

The software Fastp [34] was employed to trim sequencing adapters and remove nucleotides with a quality score below 20. For read alignment, the Burrows-Wheeler Aligner (BWA) [35] was used to map the reads to the hg19 reference genome. Following alignment, Picard tools were applied to identify and flag duplicate reads within the BAM files. The next step in post-alignment processing involved local realignment around indels to amend any misalignments. Before proceeding to variant calling, a base quality score recalibration was conducted to mitigate systematic errors. Mutect2 [36] was then used for the joint calling of somatic single nucleotide variants (SNVs) and insertions/deletions (InDels). ANNOVAR was engaged to annotate the variants with biological information [37]. Copy number variations were detected using the CNV kit [38]. The GC content of the sequences was factored in to normalize the distribution of reads, and this normalized read distribution across sliding

windows was employed to determine copy number differences between tumor and normal samples.

RNA extraction and RNA sequence analysis

The TRIzol reagent (ThermoFisher, 15596026, USA) was utilized for the extraction of total RNA, followed by purification in accordance with the manufacturer's provided protocols. Divalent cations were then used to cleave the mRNA into smaller pieces. These RNA fragments were used as templates for the synthesis of complementary DNA (cDNA) through reverse transcription. Subsequently, U-labeled second-strand DNA was synthesized using the cDNA as a template. Before the indexed adapters were attached, an additional A-base was appended to the blunt ends of the DNA strands. The fragments were then ligated with dual-index adapters and size-selected with AMPureXP beads. Post-ligation, the products were amplified by PCR, following the application of a heat-labile UDG enzyme (NEB-cat.m0280). The cDNA libraries produced had an average insert size of approximately 300 ± 50 bp. The libraries underwent sequencing using the Illumina Novaseq™6000 system (LC-Bio Technology CO., Ltd.) with a PE150 configuration, generating paired-end reads of 2 × 150 bp, in line with the vendor's provided procedures. The DESeq2 software was utilized to perform differential expression analysis of genes, comparing two distinct groups. For comparing two samples, edgeR was employed. When comparing two individual samples, edgeR was the tool of choice. Genes that demonstrated a false discovery rate (FDR) less than 0.05 and an absolute fold change exceeding 2 were categorized as differentially expressed. These identified genes then underwent enrichment analysis through Reactome pathways, Gene Ontology (GO) functions, and Kyoto Encyclopedia of Genes and Genomes (KEGG) pathways.

MSCs isolation and culture

MSCs were extracted from the human placenta using the same method described in previous studies [39, 40]. These MSCs were subsequently cultivated in Petri dishes using a DMEM medium (Gibco-Invitrogen) containing 10% FBS, along with a combination of antibiotics.

Production of viral vectors and transduction

The MSCs were incubated in a 37°C environment with 5% CO_2, using DMEM supplemented with 10% FBS and a dual antibiotic solution containing penicillin/streptomycin at a concentration of 50 U/ml. Lentiviral vectors were created using the pLKO.1-TRC (Addgene, #10878), psPAX2 (Addgene, #12260), and pMD2.G(Addgene, #12259) plasmids to enable the expression of short hairpin RNA (shRNA) for inhibiting kindlin-2 (Sh-K2) or a non-targeting scrambled shRNA (Sh-con). The specific sequences used were as follows: Sh-K2, 5'-GAGGACC TATATGAATGG-3'; Sh-con, 5'-ACGCATGCATGCT TGCTTT-3'. Lentiviruses carrying these Sh-K2 and Sh-con were produced by co-transfecting HEK293T cells. To generate DNA expression vectors, kindlin-2 cDNA encoding the corresponding protein sequences were cloned into the 3×FLAG tagged pLVX-IRES-Hyg (3f). To generate lentiviral expression vectors encoding kindlin-2, 3×FLAG-kindlin-2(3f-K2) were co-transfected with psPAX2 and pMD2.G into HEK293T cells.

For the transduction process, MSCs or fibroblasts were grown in their standard growth medium until they achieved a cell density of 70%. Afterward, a fresh medium was introduced, which included the lentivirus at a multiplicity of infection (MOI) level of 100, and incubated for 24 h. The viral transduction was conducted with the addition of 8 μg/mL polybrene to enhance infection efficiency.

Western blot analysis

The western blot procedure was performed by methods previously reported [39, 40]. The total protein extracts were isolated using a 1% SDS lysis buffer (P0013G, Beyotime). 10 to 60 μg protein samples per lane were subjected to 10% SDS-polyacrylamide gel electrophoresis and subsequently transferred onto nitrocellulose membranes. The protein-loaded membranes were blocked for sixty minutes at room temperature using a solution comprising 5% skimmed milk. Following this, the membranes underwent an overnight incubation at 4 °C with primary antibodies: GAPDH conjugated with HRP (Santa Cruz, sc-365062HRP) and kindlin-2 (Proteintech, 11453-1-AP). After extensive washing, the membranes underwent incubation with secondary anti-rabbit antibodies (Jackson ImmunoResearch, #711-005-152) conjugated to HRP. The protein bands were detected using the Bio-Rad ECL kit, and the immunoblot was visualized using the Syngene G：BOXChemiXX9 automated digital imaging system.

CCK-8 test

The cells were processed following the procedures outlined in the "Ultra-low adsorption culture" and "MSCs isolation and culture" sections. Washed the cells with PBS which was centrifuged at 1500 rpm for 5 minutes and removed the PBS, repeated this step twice. Resuspended cells with melted Mi-gel to reach a concentration of 2×10^6 cells per milliliter gel. Then Mi-gel buffer B was added, and the ratio of Mi-gel and Mi-gel buffer B was 20:1. Fully mixed the cell suspension with a pipette. Added 10ul of cell suspension to every well in a 96-well plate for cell culture. Each group had 5–6 repetitions. After a 7-day culture, refreshed the medium and added 100ul medium, then added 10ul Cell Counting Kit-8 (C0037, Beyotime) into the wells. The plate

was incubated at 37 °C for 60 min, before measuring the absorbance at 450 nm using a microplate reader (BioTek, SYNERGYLX).

Statistical analysis

Statistical comparisons between two independent groups were conducted using two-tailed unpaired parametric Student's t-tests or Mann-Whitney test. The Pearson correlation coefficient was employed for assessing correlations. All results were presented as mean values ± SD. In the Figures, asterisks denoted statistical significance as follows: *, **, ***, and **** represent p values smaller than 0.05, 0.01, 0.001, and 0.0001 respectively; while n.s. indicates a p value larger than 0.05. The creation of graphs and the statistical analyses were performed using the software GraphPad Prism 9.0 and the R programming language for statistical computing.

Results

Co-cultivation with fibroblasts promotes the development of organoid

For the generation of LCOs within clusters were isolated from surgically excised lung cancer (LC) tissues through dissociation. These cellular components were then encapsulated within Mi-gel and submerged in a specialized medium for LCOs. By employing this methodology, we successfully preserved a total of 102 lines of LCOs, including the aforementioned 20 LCOs [33]. The cell lines were sourced from six distinct subtypes of lung cancer, encompassing squamous cell carcinoma, adenocarcinoma, adenosquamous carcinoma, lymphoepithelioma-like carcinoma (LELC), small cell carcinoma, and large cell carcinoma. A portion of these LCOs (21 out of 102) were cultivated for a prolonged duration of 4 months, during which no noticeable alterations in their spherical organoid structure were observed.

During the establishment of a lung cancer organoid model, it was observed that three cases (LCO-48, LCO-49, and LCO-59) failed to generate tumor organoids using conventional culturing methods (Fig. 1A, upper). To investigate the underlying reasons for the failure of tumor organoid formation, we isolated and cultured fibroblasts derived from the adjacent non-cancerous tissue of each sample. When the proportion of fibroblasts in the total number of cells is 10%, 20%, 30%, 40%, 50%, 60%, respectively, the effect on the formation of lung cancer tumor organoids can be observed from the results, the higher the proportion of fibroblasts, the easier the cells to gather into spheres. When the proportion of fibroblasts was 50%, the diameter of the organoids formed was significantly larger than that of the organoids formed by other proportions. Therefore, we believe that the proportion of fibroblasts in the total cells is 50%, which is an appropriate proportion to promote the formation of tumor organoids (Fig. S1A-B). In the subsequent experiments, we selected 50% fibroblasts as the experimental condition.

When co-culturing the isolated fibroblasts with their corresponding tumor cells in Mi-gel, we observed that these three samples, which initially failed to form tumor organoids, exhibited successful formation of tumor organoids upon addition of their respective fibroblasts (Fig. 1A below). A similar phenomenon was also observed in ultra-low adsorption culture (Fig. S2). After 7 days of co-culture, the CCK-8 assay demonstrated a noteworthy three-fold increase in viable cell yield for the three tumor organoids formed through co-culturing with fibroblasts (Fig. 1B-D). Collectively, our findings suggest that the inclusion of fibroblasts derived from the sample enhances multicellular aggregation and cell viability during LCO generation.

The presence of MSCs in co-culture stimulates organoid growth

MSCs have a wide range of sources, strong expansion ability, low immunogenicity, and multi-directional differentiation potential, which are of special value in medical research and clinical applications [41–43]. To assess the function of MSCs in the culture of LCOs, we conducted a co-culture of MSCs with lung cancer cells derived from patients using Mi-gel and observed that in these three samples, which were unable to form tumor organoids. The effect on the formation of lung cancer tumor organoids can be clearly observed when the proportion of MSCs ranges from 30 to 60%, similar to the addition of fibroblasts in lung cancer cells. The diameter of the organoids formed was significantly larger than that of organoids formed in a proportion of less than 30% (Fig. S3A-B). Therefore, we believe that the proportion of MSCs in the total cells is 30–60%, which is an appropriate proportion to promote the formation of tumor organoids. In the subsequent experiments, we selected 50% MSCs as the experimental condition.

The addition of MSCs resulted in the formation of lung cancer cell-derived organoids , as depicted in Fig. 2A. Following a 7-day co-culture, the CCK-8 results revealed a significant increase in the number of viable cells within the three tumor organoids co-cultured with MSCs, exhibiting an increase ranging from 2.3 to 3.4-fold compared to the control group (Fig. 2B-D). Collectively, our data suggest that the addition of MSCs promotes multicellular aggregation and cell survival during LCO generation. MSCs exert a comparable role to patient-derived fibroblasts in the formation of LCOs.

Additionally, we conducted experiments to assess whether the combination of fibroblasts and MSCs enhanced the efficacy of LCO formation. We co-cultured LCCs with MSCs, fibroblasts, or a combination of both in

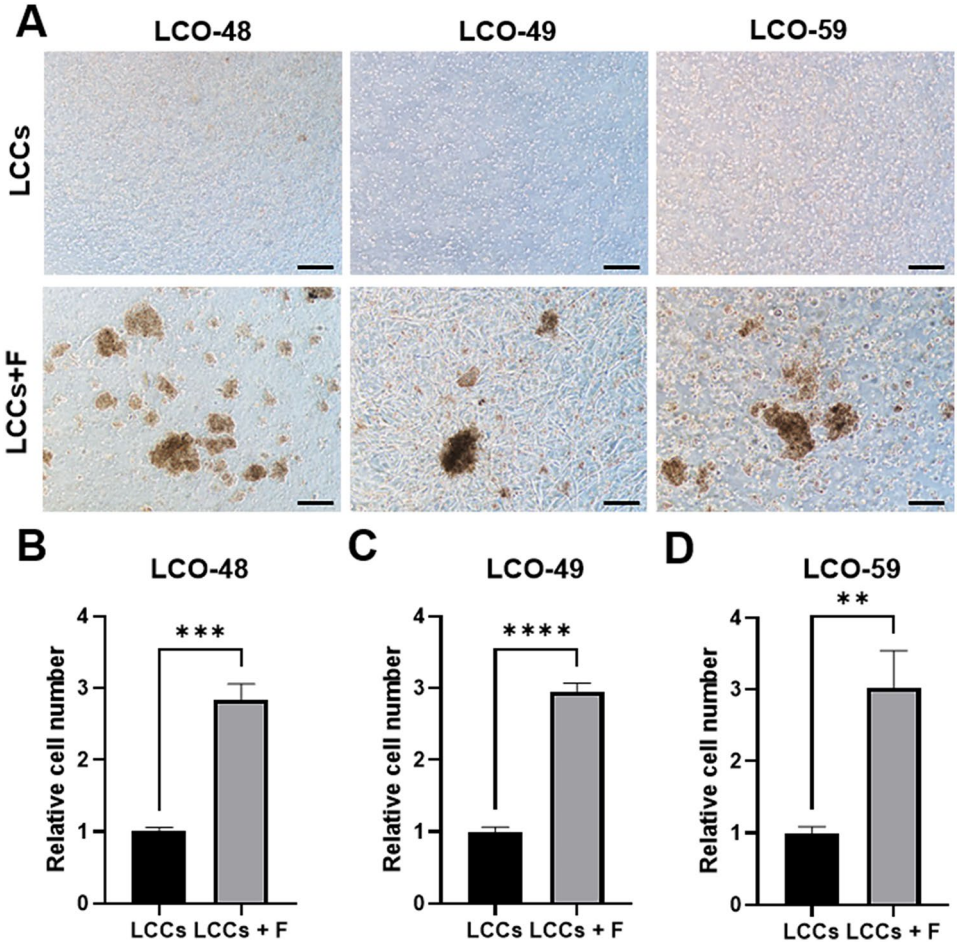

Fig. 1 Fibroblasts contribute to the formation of LCOs (**A**). LCCs were cultured with/without fibroblasts (F) and observed under bright-field microscopy after 2 weeks of culture. The scale bar represents 200 μm. (**B**-**D**) The number of viable cells in LCOs from three different patients was compared after a culture period of 7 days. The data are represented as the mean ± SD. Values with a $p < 0.05$ were considered statistically significant as per the Student's t-test, ** $p < 0.01$, *** $p < 0.001$,**** $p < 0.0001$. LCCs: patient-derived lung cancer cells

equal proportions. Interestingly, we observed that the co-culture of LCCs with MSCs resulted in the largest diameter of formed LCOs. However, there was no significant difference in cell proliferation among the different groups (Fig. S4A-B).

LCOs reproduce the histological properties of the primary tumor

Maintaining the histological traits of the originating tumor in LCOs is crucial, especially when they are co-cultured with fibroblasts obtained from the identical sample. To evaluate the morphological and histological similarities between LCOs and the initial lung cancer specimens, we employed HE and IF staining techniques. LELC, an uncommon variant of non-small cell lung cancer, is typically characterized by dense infiltration of lymphocytes (Fig. 3A). The LCO-48, which originated from LELC, preserved the expression of characteristic LELC markers encompassing thyroid transcription factor 1 (TTF-1), CK5/6, and P63 (Fig. 3A). TTF-1 is usually positively expressed in lung adenocarcinoma cells; however, TTF-1 is usually negative for LELC. P63, an epithelial transcription factor, and CK5/6, a group of proteins that belong to the cytokeratin family, are expressed in a variety of epithelial tumors.

LCO-49 derived from lung large cell carcinoma showed large tumor cells with diverse morphology, large and irregular nuclei, prominent nucleoli, and sometimes multinucleated giant cells, similar to its parental cancer tissue (Fig. 3B). And maintained the expression of lung large cell carcinoma markers, including BRG1, CD56, CK18, and Synaptophysin (syn) (Fig. 3B). In LCO-59, the squamous cells exhibited distinct cell margins and keratinization within the cytoplasm, hallmarks of the histological presentation of lung squamous cell carcinoma. Furthermore, markers characteristic of squamous cell carcinomas, such as P63 and CK5/6, were found to be elevated, whereas TTF-1 was not detected (Fig. 3C).

Actin and integrin β1, highly conserved proteins present in all eukaryotic cells, play a fundamental role in cell

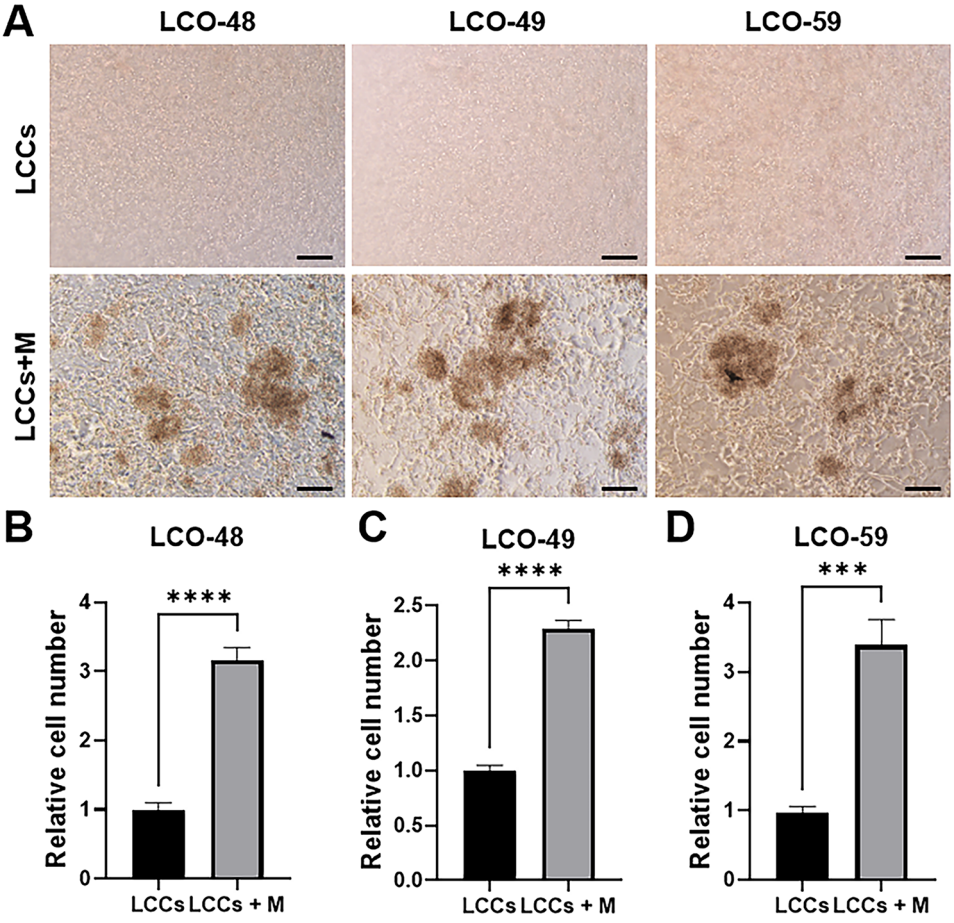

Fig. 2 MSCs contribute to the formation of LCOs. (**A**) LCCs were incubated either alone or with MSCs (M). Images captured using bright-field microscopy show LCOs after a culture duration of 2 weeks. The scale bar represents 200 μm. (**B**-**D**) The number of live cells in LCOs from three individual patients was compared following a 7-day culture period. The data are presented as the mean ± standard deviation. The Student's t-test was used to determine statistical significance, with p values less than 0.05 considered significant, *** $p < 0.001$, **** $p < 0.0001$

morphology. To visualize cellular structure, we assessed the expression of F-actin and integrin β1 as markers for cytoskeleton and basal membranes, respectively. Both actin and integrin β1 were found to be strongly expressed in lung cancer specimens and LCOs (Fig. S5), indicating that LCOs maintain the cell structural characteristics of their parent lung cancer (LC) specimens. Subsequently, we examined the distribution of proliferating cells within the organoids. Our findings revealed that proliferative cells were dispersed throughout the entire cellular mass of the organoid in LCOs. This observation is consistent with the diffuse staining pattern of Ki67 observed in primary tumors (Fig. S5). Collectively, these findings imply that the histological structure and marker expression have been accurately reproduced from the original lung cancer tissue in the LCOs.

LCOs maintain the genetic mutation profile of the source tumor

To evaluate if LCOs co-cultured with fibroblasts derived from the same patient maintain the original gene mutations of their source tumors, WES was conducted on three matched sets of primary lung cancer specimens and their respective LCOs. The results showed that LCOs retained most of the variants in their original cancer tissues, such as PRDM2, NFKBIA, BCLAF1, and PDE4DIP, which were largely conserved between the organoid cell line and the primary tumor (Fig. 4A). The scatter plot depicting the variant allele frequency (VAF) observed within these organoids typically mirrors that observed in the initial cancerous tissue (Fig. 4B). The somatic mutations of cancer-associated genes in LCOs and matched lung cancer tissue encompassed various types, including missense mutations, frameshift deletions, and splice site alterations. In the analyzed samples, most somatic mutations in LCOs consistently exhibited a high degree of concordance with the corresponding lung cancer

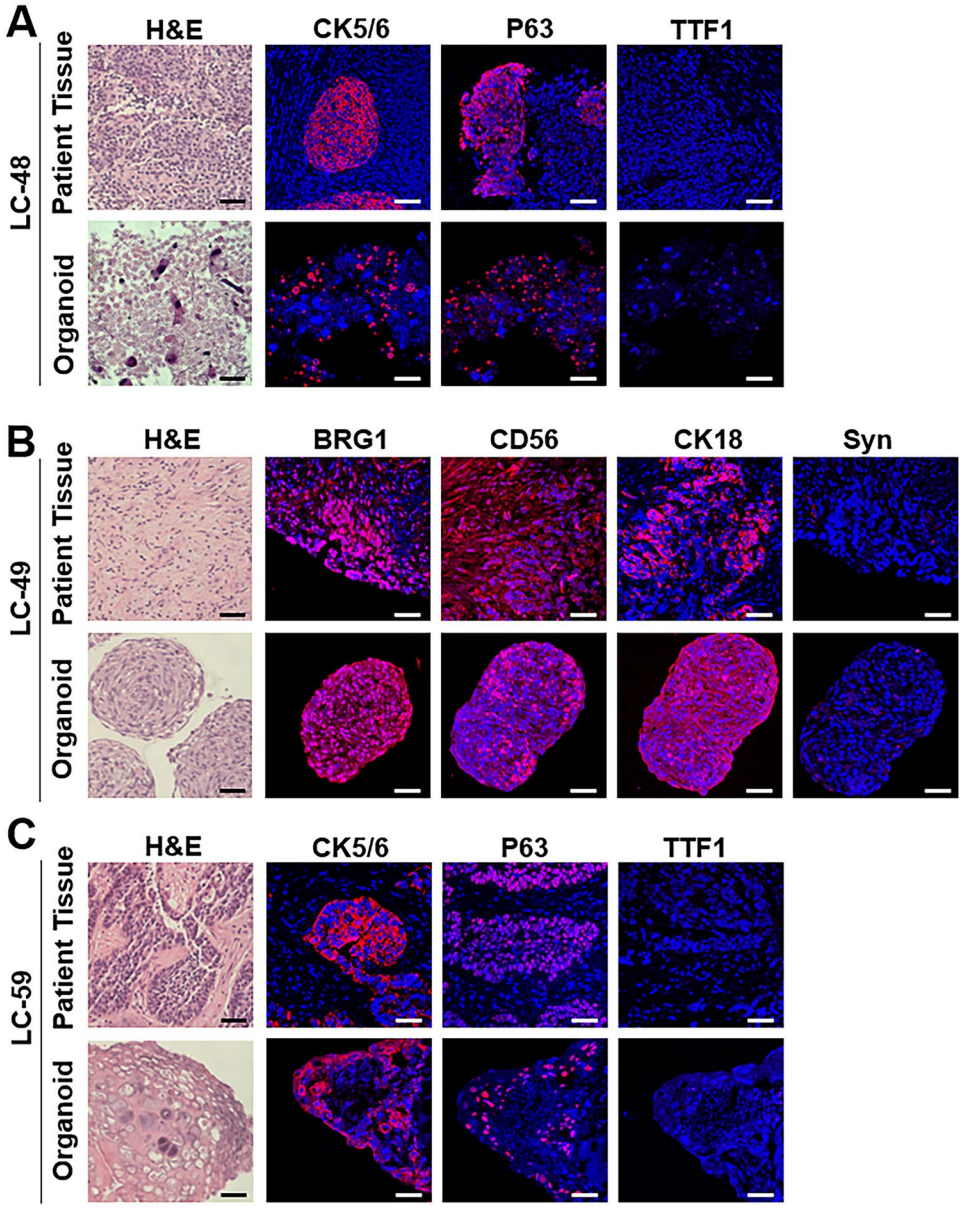

Fig. 3 LCOs mirror the properties of the source tissues. Organoids LCO-48 (**A**) originating from pulmonary lymphoepithelioma-like carcinoma, LCO-49 (**B**) from lung large cell carcinoma, and LCO-59(**C**) from lung squamous cell carcinoma, along with their respective original tumor tissues, were subjected to H&E staining and immunofluorescence analysis. The nuclei were stained with DAPI (blue), and the immunofluorescence images displayed are representative (red). The scale bar represents 50 μm

tissues; while a minority of them displayed a variable pattern of alteration (Fig. 4C). By comparing the Ti and Tv of LCOs and matched lung tumor samples, similar tumor mutation profiles were reflected (Fig. 4D). To further investigate the fidelity with which LCO cell lines preserve mutational characteristics from their progenitor tumors, we examined patterns of somatic mutations in both tumor specimens and organoids cultured on various substrates. The proportion of base somatic mutation patterns in lung cancer tissues was well maintained in corresponding LCOs (Fig. 4E).

Differential expression of genes in LCOs and paracancerous organoids (POs)

To evaluate the variations in gene expression profiles between LCOs co-cultured with fibroblasts and POs, RNA sequencing was performed on 3 groups of LCOs and POs. The heatmap of gene expression groups genes together according to the resemblance of their expression patterns among the different samples, providing a visual representation of gene activity in different samples. This visualization reveals substantial disparities in the gene expression profiles between LCOs and POs (Fig. 5A).

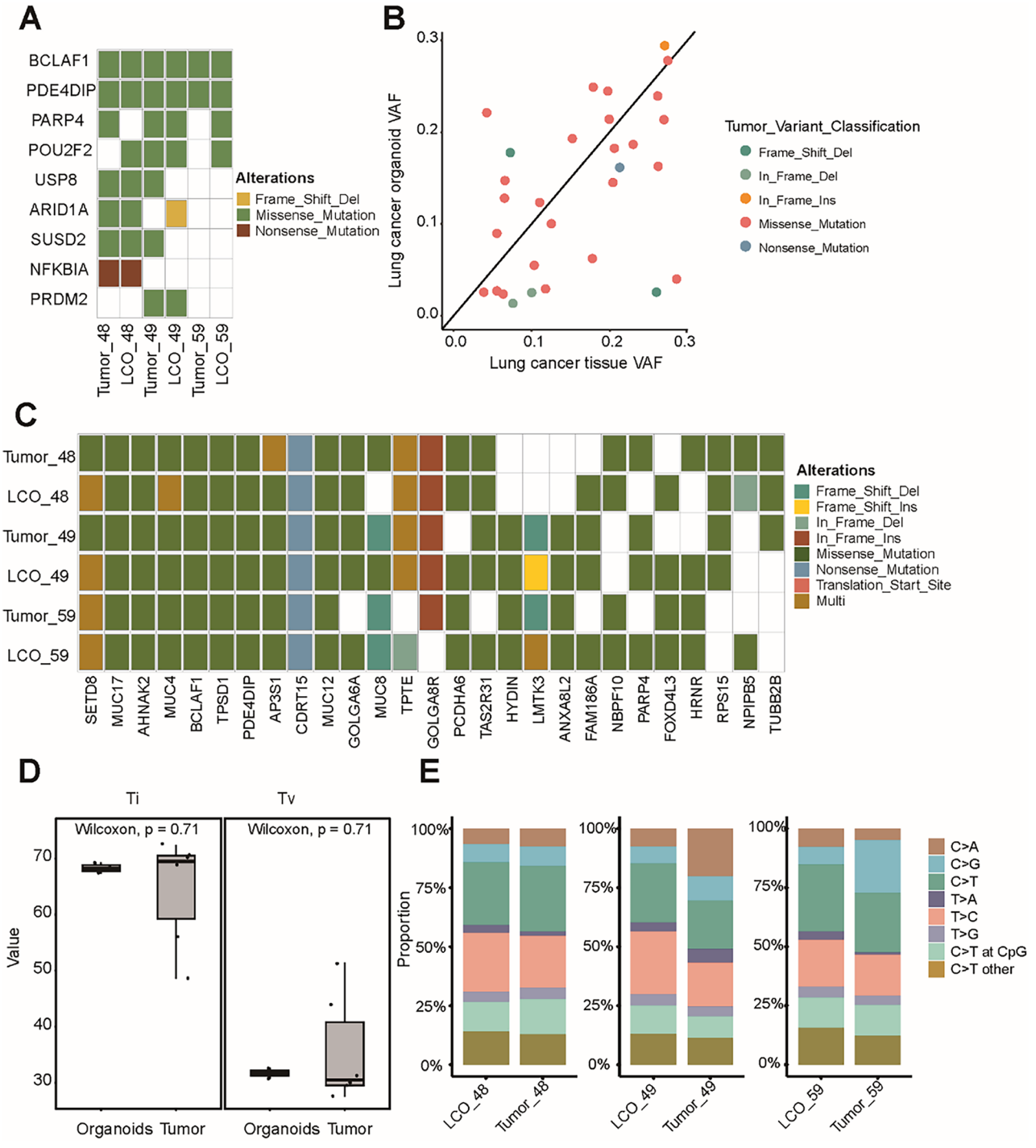

Fig. 4 LCOs maintain the genetic profile of the original tumor tissues. (**A**) A heatmap illustrates the somatic mutations in cancer-related genes found in LC tissues and their corresponding LCOs. (**B**) The VAF of genetic changes in LCOs is compared with that in LC tissues. (**C**) A heatmap details the most prevalent 27 mutations in LCOs alongside their matching LC tissues. (**D**) The ratio of C > T/G > A transitions (Ti) to C > A/G > T transversions (Tv) is compared between organoids and their tumor counterparts. The data are represented as the mean ± standard deviation. The Wilcoxon test was used to determine statistical significance for p values less than 0.05. (**E**) The chart shows the distribution of exonic variants in LCOs versus the original tumors, with the six types of nucleotide substitutions detailed in the legend

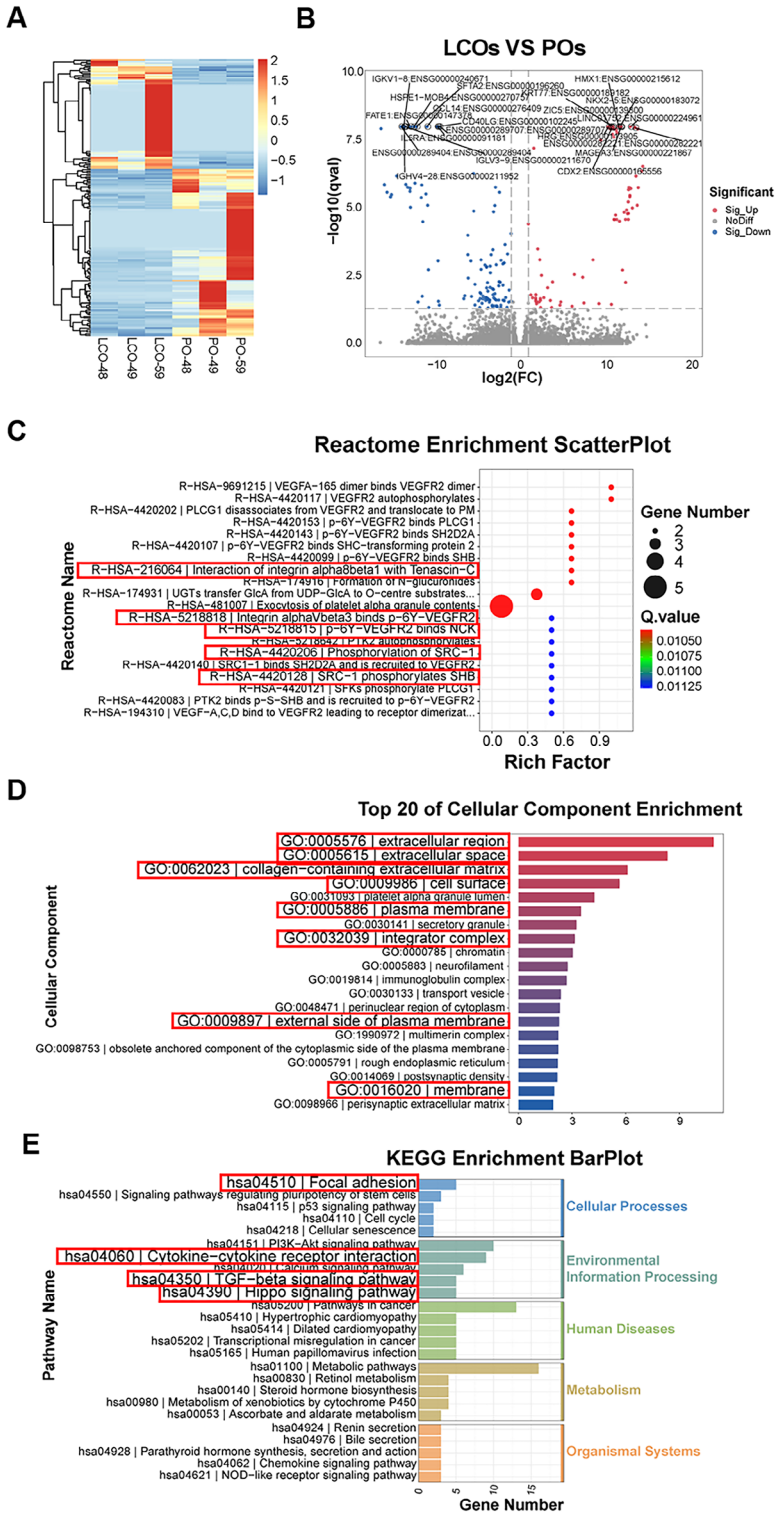

Fig. 5 Gene expression profiles in LCOs compared to POs (**A**). Heat maps display the gene expression differences between LCOs and their respective POs. (**B**) A volcano plot highlights genes with differential expression between LCOs and POs, with significant genes marked in blue (downregulated) and red (upregulated), while non-significant changes are in gray. (**C**) A bubble chart for Reactome pathway enrichment shows the rich factor, which is the proportion of differentially expressed genes in a pathway relative to the pathway's total gene count. The q value represents the adjusted p value. Dot colors and sizes indicate the q value range and the count of differentially expressed genes in the pathways, respectively. (**D**) Bar chart of the top 20 differentially expressed genes from Gene Ontology (GO) cellular component enrichment analysis in LCOs and POs. (**E**) Bar chart of Kyoto Encyclopedia of Genes and Genomes (KEGG) pathway analysis for differentially expressed genes in LCOs and POs

The general landscape of differentially expressed genes can be grasped through volcano plot visualization. Figure 5B displays the top 20 genes that show the most significant differences in expression. The results of the reactome pathway enrichment analysis were visualized using a bubble chart. The bubble plot illustrates the 20 pathways that exhibit the lowest Q values (Fig. 5C). Our results suggest that LCOs exhibit a higher enrichment of integrin-related signaling pathways and potential interacting proteins compared to POs. After conducting an analysis using Gene Ontology, it was observed that notably altered genes in LCOs displayed significant enrichment of the top 20 cellular components in extracellular regions, extracellular space, and collagen-related ECM, which are known to be regulated by integrin-mediated signaling pathways (Fig. 5D). Furthermore, KEGG analysis of differentially expressed genes between LCOs and POs identified significant disparities in focal adhesion pathways as well as downstream-regulated TGF-β and Hippo signaling pathways (Fig. 5E), suggesting their pivotal role in shaping the microenvironment during LCO development.

Kindlin-2 mediated fibroblasts/MSCs promote organoid formation

Through the above differential expression analysis of genes in LCOs and their corresponding POs, we have identified that the integrin-related signaling pathway and downstream focal adhesion proteins may have an impact on the regulation of the culture of LCOs. Subsequently, we examined the functional importance of kindlin-2 within the culture of LCOs, given its pivotal role as a regulator protein in integrin signaling and ECM remodeling. We employed sh-Kindlin-2 lentiviruses to reduce the expression levels of kindlin-2 in fibroblasts (Fig. S6) and subsequently conducted a co-culture with patient-derived LCCs. The number and volume of LCOs with kindlin-2 knockdown exhibited a significant decrease compared to those in the control group (Fig. 6A-B). After 7 days of co-culture, organoid structures emerged within the system. The viability of the three LCOs with kindlin-2 knockdown in fibroblasts was significantly diminished in comparison to the control group, according to the results of the CCK-8 assay (Fig. 6C).

We also made the same attempt in the LCO formation experiment of MSC co-culture. We employed sh-Kindlin-2 lentiviruses to reduce the expression levels of kindlin-2 in MSCs (Fig. S7A) and subsequently conducted a co-culture with patient-derived LCCs. The number and volume of LCOs with kindlin-2 knockdown exhibited a significant decrease compared to those in the control group (Fig. 7A-B and S7B). After 7 days of co-culture, organoid structures emerged within the system. The viability of the three LCOs with kindlin-2 knockdown in MSCs was significantly diminished in comparison to the control group, according to the results of the CCK-8 assay (Fig. 7C).

To further analyze the regulatory effect of kindlin-2 on LCO formation, We employed 3f-Kindlin-2 lentiviruses to overexpression kindlin-2 in MSCs (Fig. S8) and subsequently conducted a co-culture with patient-derived LCCs. Overexpression of kindlin-2 in MSCs significantly increased organoid size (Fig. 8A-B) and partially organoid number (Fig. 8C). The findings suggest that kindlin-2 mediated MSC plays a pivotal role in the development of lung tumor organoids, highlighting the significance of kindlin-2 as a key regulator within the TME of these organoids.

LCOs maintain drug sensitivity

We then assessed the practicality of three LCOs (LCO-48, LCO-49, and LCO-59) for conducting drug susceptibility testing. These organoids were subjected to co-culture with fibroblasts or MSCs, which were then exposed to various concentrations of commonly employed drugs for lung cancer treatment comprising 5-FU, cisplatin, and doxorubicin. The patient-derived lung cancer cells were cultured and allowed to grow for a week, after which they were exposed to the drugs for 3 days. The viability of the cells was assessed using the CCK-8 assay kit. The assessment of drug sensitivity was conducted by measuring the relative viability of cells, and the corresponding IC50 values were calculated. Consistent trends were observed between LCOs (co-culture with fibroblasts or MSCs) and corresponding sample tumor cells for each drug, indicating similar chemosensitivity of LCOs and lung cancer cells (Fig. 9A-C). Notably, the sensitivity to chemotherapeutic agents may vary among different subtypes of non-small cell lung cancer (NSCLC), such as LELC, lung large cell carcinoma, and lung squamous cell carcinoma, due to various factors including tumor molecular biology, patient-specific differences, and gene expression profiles. For instance, the sensitivity of LCO-48 and LCO-59 to doxorubicin and 5-FU was higher compared to that of LCO-49 (Fig. 9A-C), whereas LCO-59 exhibited low sensitivity to cisplatin (Fig. 9C).

Next, we investigated whether LCOs retained their sensitivity to therapy compared to parental tumor cells, thus making them a valuable tool for ascertaining individualized chemotherapy regimens. When LCCs derived from patient 49#, who received postoperative adjuvant therapy with etoposide and cisplatin in the clinic, were co-cultured with fibroblasts or MSCs and subsequently treated with 10 μm of either etoposide or cisplatin alone, or their combination respectively, we observed that these organoids exhibited similar drug sensitivity as patient-derived LCCs (Fig. 9D). Furthermore, this drug combination also demonstrated a comparable effect in clinical treatment.

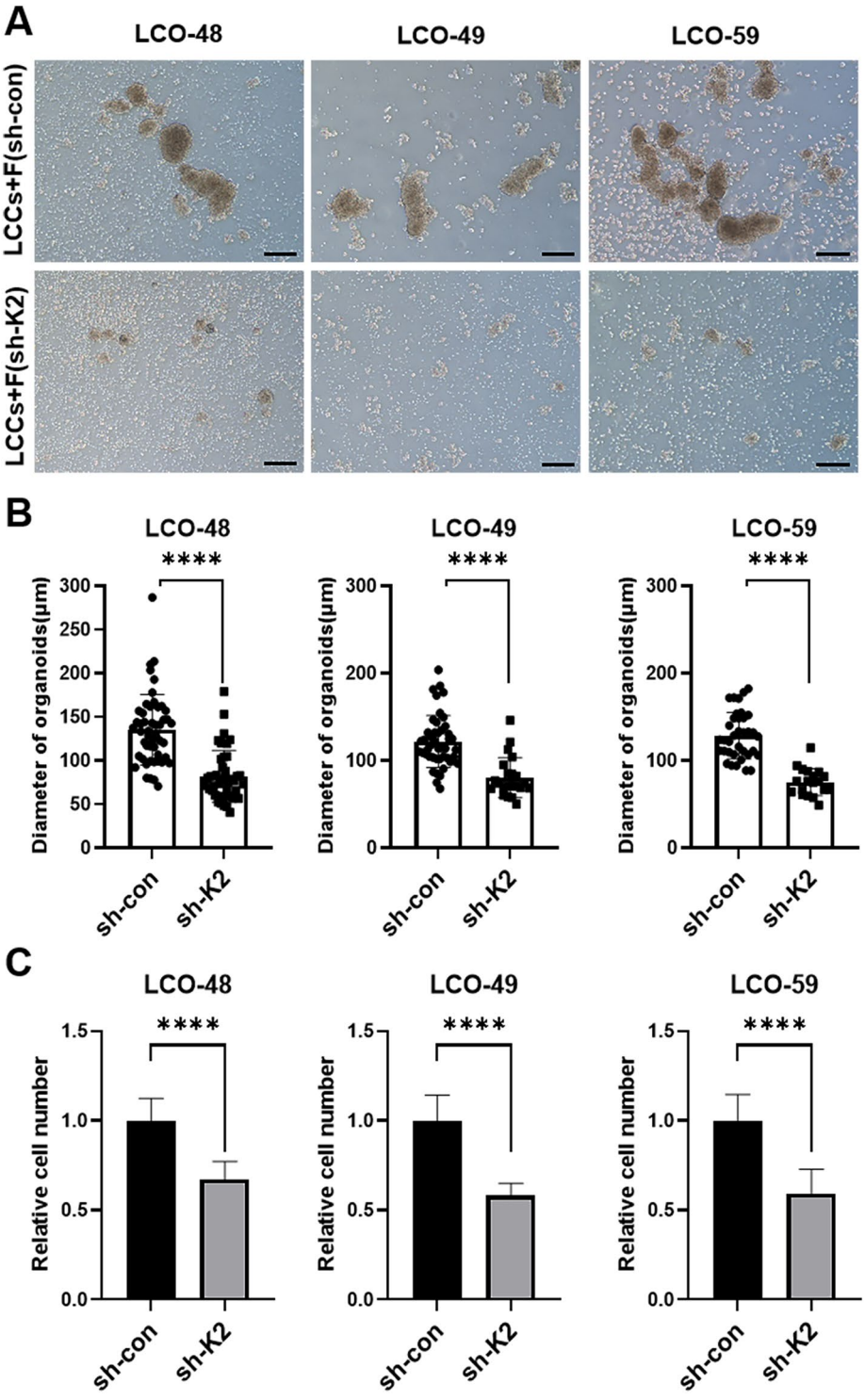

Fig. 6 Downregulation of Kindlin-2 in fibroblasts reduces organoid formation. (**A**-**C**) Primary cells derived from lung cancer were cultured with sh-con (control shRNA) fibroblasts or sh-K2 (sh-kindlin-2) fibroblasts. Fibroblasts were transduced with lentiviral vectors carrying sh-K2 or sh-con and then cultured for 5 days. Bright-field images illustrate the LCOs produced by the co-culture of these fibroblasts with LCCs (**A**) and provide quantification of the size of the LCOs (**B**). The scale bar represents 200 μm. (**C**) The viability of cells in LCOs from three patients after a 7-day culture period was compared. The data are expressed as the mean ± SD. The Mann-Whitney test was used to assess statistical significance for p values less than 0.05, **** $p < 0.0001$

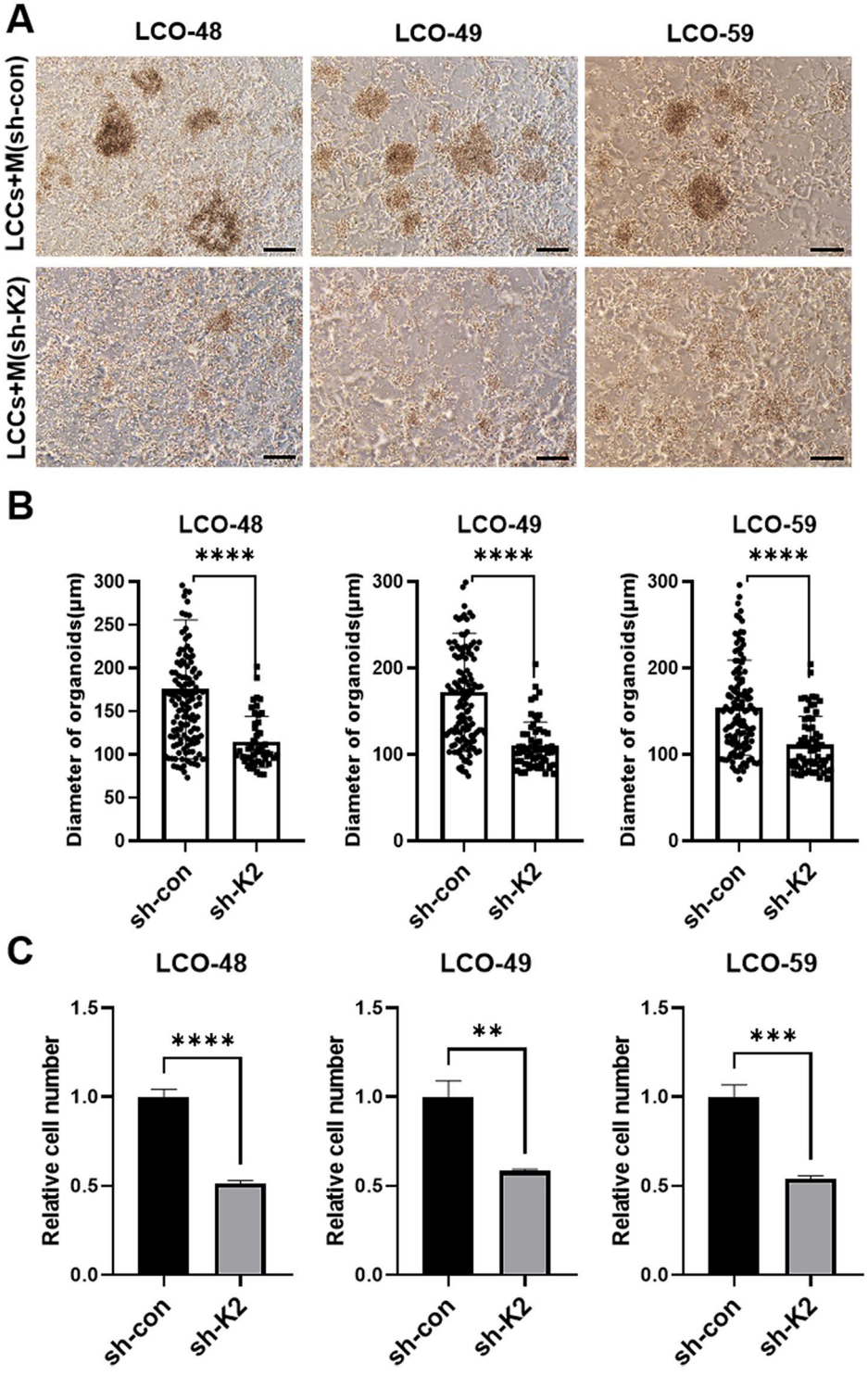

Fig. 7 Downregulation of Kindlin-2 in MSCs reduces organoid formation. (**A**-**C**) Primary cells derived from lung cancer were cultured with sh-con (control shRNA) MSCs or sh-K2 (sh-kindlin-2) MSCs. MSCs were transduced with lentiviral vectors carrying sh-K2 or sh-con and then cultured for 5 days. Bright-field images illustrate the LCOs produced by the co-culture of these MSCs with LCCs (**A**) and provide quantification of the size of the LCOs (**B**). The scale bar represents 200 μm. (**C**) The viability of cells in LCOs from three patients after a 7-day culture period was compared. The data are expressed as the mean ± SD. The Mann-Whitney test was used to assess statistical significance for p values less than 0.05, ** $p < 0.01$, *** $p < 0.001$, **** $p < 0.0001$

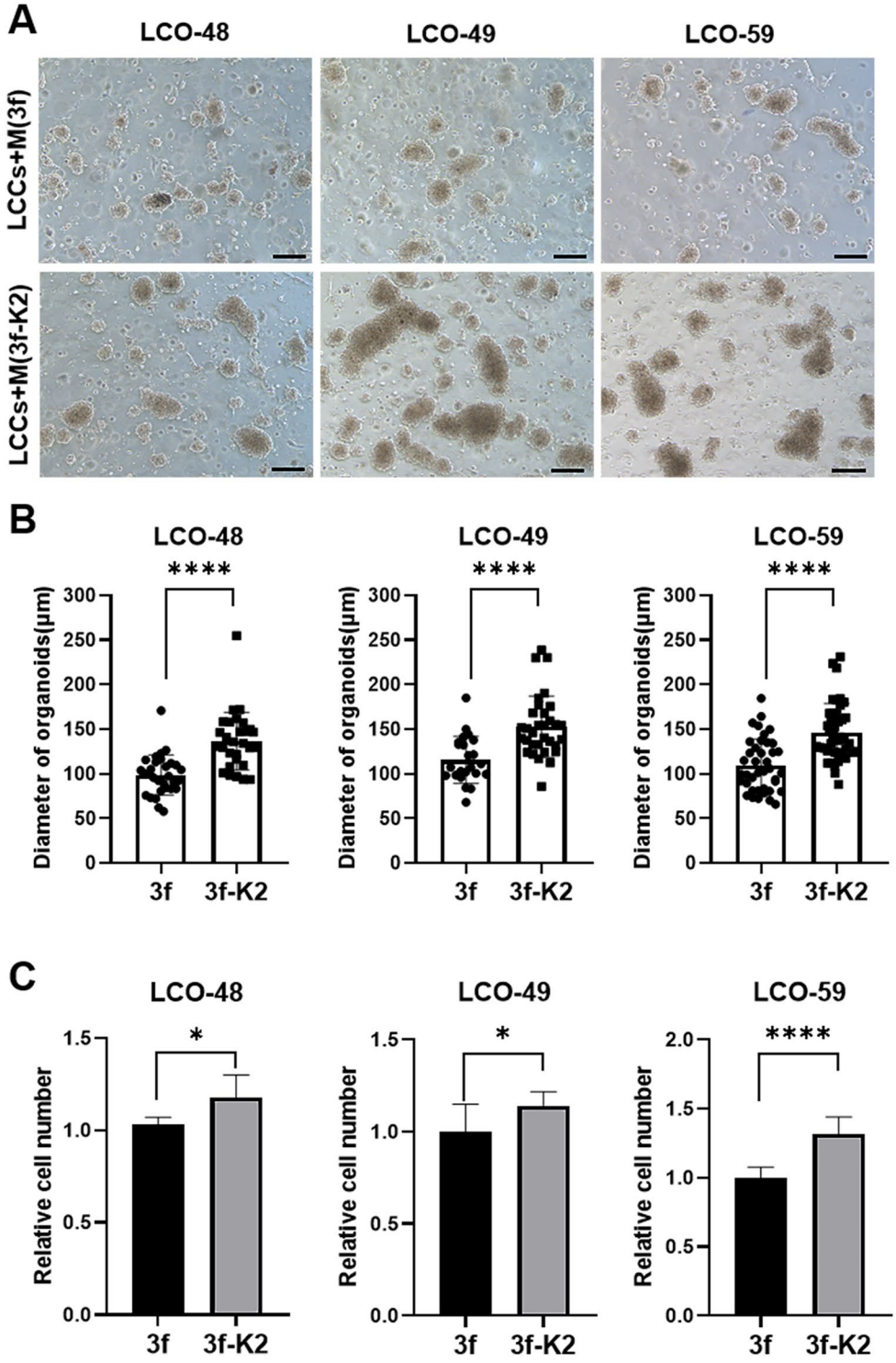

Fig. 8 Kindlin-2 mediated MSCs promote organoid formation. (**A**-**C**) Primary cells derived from lung cancer were cultured with 3f MSCs or 3f-K2 (3f-kindlin-2) MSCs. MSCs were transduced with lentiviral vectors carrying 3f-K2 or 3f and then cultured for 5 days. Bright-field images illustrate the LCOs produced by the co-culture of these MSCs with LCCs (**A**) and provide quantification of the size of the LCOs (**B**). The scale bar represents 200 μm. (**C**) The viability of cells in LCOs from three patients after a 7-day culture period was compared. The data are expressed as the mean ± SD. The Mann-Whitney test was used to assess statistical significance for p values less than 0.05, * $p < 0.05$, **** $p < 0.0001$

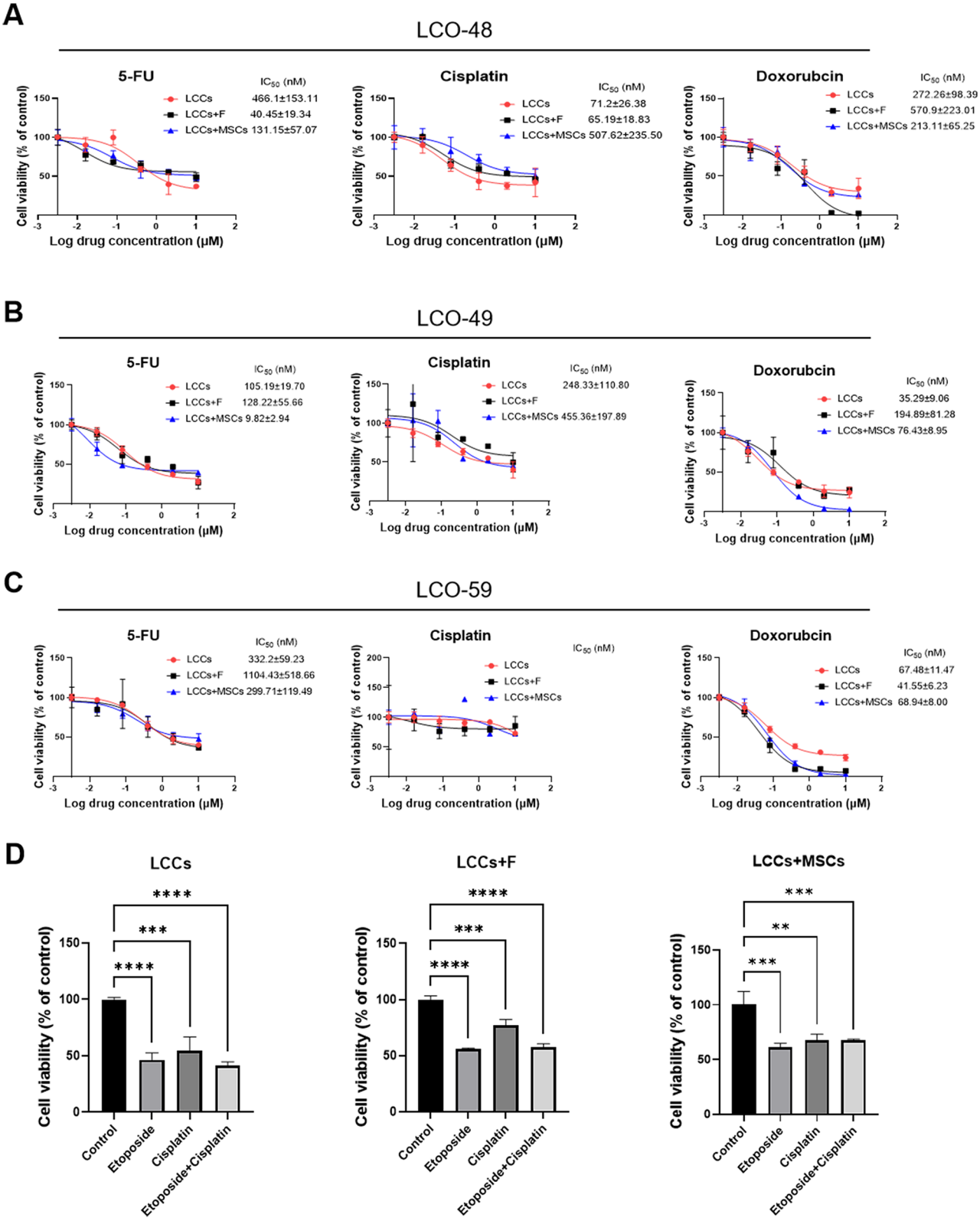

Fig. 9 (See legend on next page.)

(See figure on previous page.)

Fig. 9 Drug testing of LCOs. (**A**) Dose-response curves after 3 days of treatment with indicated drug concentrations of 5-FU, cisplatin and doxorubicin in LCO-48 with fibroblasts (F) or MSCs) and paired LCCs derived from patients. (**B**) Dose-response curves after 3 days of treatment with indicated drug concentrations of 5-FU, cisplatin and doxorubicin in LCO-49 with fibroblasts (F) or MSCs) and paired LCCs derived from patients. (**C**) Dose-response curves after 3 days of treatment with indicated drug concentrations of 5-FU, cisplatin, and doxorubicin in LCO-59 with fibroblasts (F) or MSCs) and paired LCCs derived from patients. The cell viability was measured by cell number. (**D**) The drug sensitivity of these organoids was similar to that of patient-derived LCCs. When LCCs and LCOs (LCO-49) co-cultured with fibroblasts or MSCs were treated with 10 μm etoposide or cisplatin, respectively, or their combination for 3 days. The viability of cells was compared. The data are expressed as the mean ± SD. The one-way ANOVA was used to assess statistical significance for p values less than 0.05, ** $p < 0.01$, *** $p < 0.001$, **** $p < 0.0001$

Therefore, the susceptibility of this in vitro co-culturing model can be effectively utilized for determining personalized chemotherapy treatments.

Discussion

Tumor organoids are in vitro cultured three-dimensional cellular constructs that replicate the microenvironment and cell diversity of real tumors. The efficiency of cultivating tumor organoids is influenced by factors such as the type of tumor, the methods of sample collection and handling, and the conditions of the culture environment, among others. Specifically, the culture success rate for organoids derived from patients with hepatocellular carcinoma is below 30% [44, 45], which constrains their utility in the field of precision oncology. Several studies have shown that the success rate of LCOs can be up to more than 80%, and there is a marked difference in the composition of the medium [46, 47]. Although in our culture system, the success rate of LCOs culture was already high, exceeding 90%. However, some patient-derived lung cancer cells still fail to form organoids in vitro. Therefore, exploring the molecular underpinnings of tumor organoid generation and innovating novel culture techniques hold substantial scientific and clinical significance.

The complexity of TME is diverse, posing difficulties in fully mimicking the interplay between tumor cells and other cellular constituents like MSCs, immune cells, fibroblasts, and vascular cells. Therefore, our study has focused on MSCs and fibroblasts, crucial constituents of TME that engage in various interactions with tumor cells. Therefore, by adding a certain proportion (30–60%) of MSCs or patient-derived fibroblasts, we can effectively make the tumor cells that cannot form organoids successfully form LCOs, and the results were verified in more than one culture method (Figs. 1 and 2 and S1-3). At the same time, our method can effectively promote cell aggregation and the expansion and growth of LCOs. The LCOs closely matched the original clinical samples regarding both genetic and phenotypic characteristics, effectively encapsulating the distinct genetic and molecular attributes of the tumors from individual patients (Figs. 3 and 4). Moreover, the LCOs preserved a level of drug responsiveness akin to that of the primary lung cancer cells (Fig. 9). In the tumor organoid model, the addition of fibroblasts can not only increase the survival rate of LCOs but also increase the complexity of the model and make it closer to the actual TME.

MSCs and fibroblasts coexist within TME, with MSCs possessing the capacity to evolve into fibroblasts. Evidence from studies conducted in vitro [25]as well as in vivo [48] suggests that CAFs may arise from MSCs. MSCs and CAFs exhibit numerous commonalities [49]. In an appropriate environment, efficient chemotaxis of MSCs can be driven, and induce stable differentiation of MSC-derived CAFs through a TGFβ (TGFB1) and contractility-driven mechanism [50]. Furthermore, a hypothesis suggests that fibroblasts are dormant mesenchymal cells capable of undergoing a transition into MSCs given certain circumstances [51]. In this study, we found that LCOs could be formed in all three samples that had previously failed to form organoids after co-culturing patient-derived lung cancer cells with MSCs in vitro (Fig. 2 and S3). These results suggest that MSCs have the potential to support organoid development with intrinsic properties consistent with CAFs and promote cellular interactions required for organoid formation by actively secreting factors that regulate the TME. Co-culturing tumor cells with MSCs allows for the replication of cell-to-cell interactions within the TME, which is important for studying tumor biology and drug screening. Given that MSCs can replace patient-derived fibroblasts as a crucial component in tumor organoid culture, the integration of MSCs into tumor organoid co-culture models would represent a valuable preclinical tool for investigating clonal evolution and advancing precision medicine.

Subsequently, we delve into the mechanism through which MSCs facilitate lung cancer organoid development. Our research has pinpointed genes that are expressed differently between LCOs and POs, uncovering the significant influence of the integrin-linked signaling pathway in the progression of LCOs (Fig. 5). Kindlin-2, as a member of the kindlin protein family, can interact with integrinβ protein to activate integrin molecules, thereby allowing cell adhesion and extension and initiating the transmission of integrin signaling pathway [52, 53]. More importantly, our recent investigation has revealed that kindlin-2 links the ECM mechano-environment with proline biosynthesis, thereby playing a pivotal role in macromolecular synthesis, redox homeostasis maintenance, and ECM remodeling [26]. In this research, we confirmed the significant contribution of kindlin-2

in facilitating the development of LCOs by employing a co-culture model with MSCs. When kindlin-2 expression was down-regulated in fibroblasts or MSCs, the number and size of LCOs formed were significantly reduced, and cell proliferation was also significantly affected (Figs. 6 and 7). Overexpression of kindlin-2 in MSCs increased the LCO size and number in co-culture (Fig. 8). Thus, kindlin-2 high expression may contribute to LCOs formation and maintenance. Future studies in LCOs culture models may provide an entirely new window to elucidate the role of the kindlin-2 pathway, as well as other signals, in cancer progression.

Conclusion

In summary, our innovative approach of co-culturing patient-derived lung cancer cells with either MSCs or fibroblasts effectively overcomes the constraint of patient-derived lung cancer cells in forming in vitro organoids, at least in part. The LCOs developed in this model successfully recapitulated the histological and genetic profile of their parental lung cancer subtypes. Furthermore, they preserved the genomic diversity observed in the original tumor tissue, as confirmed by WES comparisons with matched parental tumors. Importantly, LCOs also retained sensitivity to therapy compared to parental tumor cells, making them a valuable tool for personalized chemotherapy treatments. Notably, we identified differentially expressed genes between LCOs and POs, revealing kindlin-2 mediated signaling that may contribute to both the formation of organoids and the pathogenesis/progression of lung cancer.

Supplementary Information

The online version contains supplementary material available at https://doi.org/10.1186/s13287-024-04128-x.

Supplementary Material 1

Supplementary Material 2

Acknowledgements
The authors declare that they have not use AI-generated work in this manuscript.

Author contributions
Z. S., X. W., J. W. and S. T. conducted the experiments. X. W. and L. G. performed data analysis. C. W. and C. Z. contributed to the design of some of the experiments. Z. Y., X. W. and L. G. designed the experiments and wrote the paper. All authors reviewed and approved the final manuscript.

Funding
The study received financial support from the National Key R&D Program of China (2019YFA0906000), the Shenzhen Medical Research Fund (D2301001，B2402032), the National Natural Science Foundation of China (82273308, 82472934), the Guangdong Basic and Applied Basic Research Foundation (2021A1515111132), the Shenzhen Science and Technology Program (JHZ20220913142804008; JCYJ20220530112817040 and ZDSYS20220606101604009), the Shenzhen Key Medical Discipline Construction Fund (No. SZXK075), and the Sanming Project of Medicine in Shenzhen (SZSM202211011). This work is also sponsored by the National Cancer Center/National Clinical Research Center for Cancer/Cancer Hospital & Shenzhen Hospital, Chinese Academy of Medical Sciences and Peking Union Medical College E010122002, and the Shenzhen High-level Hospital Construction Fund.

Data availability
All the data associated with our findings are available upon request to the corresponding author. The RNA sequencing data was published in the Sequence Read Archive (SRA) and the SRA accession number is SUB14685080. Uncropped western blottings for Figs. S6, S7A and S8 are provided in Supplementary Fig. S9.

Declarations

Ethics approval and consent to participate
All procedures were approved by the Ethics Committee of Cancer Hospital & Shenzhen Hospital, Chinese Academy of Medical Sciences. The research project titled "Construction of mechanistic tumor organoid based on ECM-mediated proline metabolism" was approved on November 15, 2023 (No. KYKT2023-22-1). Patients or their guardian(s)/legally authorized representative(s) provided written informed consent for their participation in the study and the use of their tissue.

Consent for publication
Not applicable.

Competing interests
The authors report no conflicts of interest in this work.

Author details
[1]Shenzhen Key Laboratory of Epigenetics and Precision Medicine for Cancers, Department of Thoracic Surgery, National Cancer Center/National Clinical Research Center for Cancer/Cancer Hospital & Shenzhen Hospital, Chinese Academy of Medical Sciences and Peking Union Medical College, Shenzhen 518116, China
[2]College of Pharmacy, Shenzhen Technology University, Shenzhen 518118, China
[3]Institute of Scientific Instrumentation, Shenzhen Institute of Advanced Technology, Chinese Academy of Sciences, Shenzhen 518055, China
[4]Department of Biology, and Academy for Advanced Interdisciplinary Studies, Southern University of Science and Technology, Shenzhen 518055, China
[5]Department of Pathology, University of Pittsburgh School of Medicine, Pittsburgh, PA 15261, USA

Received: 26 August 2024 / Accepted: 21 December 2024
Published online: 09 January 2025

References

1. Jacob F, Salinas RD, Zhang DY, Nguyen PTT, Schnoll JG, Wong SZH, et al. A patient-derived Glioblastoma Organoid Model and Biobank recapitulates Inter- and intra-tumoral heterogeneity. Cell. 2020;180(1):188–e20422.
2. Ding S, Hsu C, Wang Z, Natesh NR, Millen R, Negrete M, et al. Patient-derived micro-organospheres enable clinical precision oncology. Cell Stem Cell. 2022;29(6):905–e176.
3. Li X, Francies HE, Secrier M, Perner J, Miremadi A, Galeano-Dalmau N, et al. Organoid cultures recapitulate esophageal adenocarcinoma heterogeneity providing a model for clonality studies and precision therapeutics. Nat Commun. 2018;9(1):2983.
4. Shi R, Radulovich N, Ng C, Liu N, Notsuda H, Cabanero M, et al. Organoid cultures as preclinical models of Non-small Cell Lung Cancer. Clin Cancer Res. 2020;26(5):1162–74.
5. Yoshida GJ. Applications of patient-derived tumor xenograft models and tumor organoids. J Hematol Oncol. 2020;13(1):4.
6. Xu S, Tan S, Guo L. Patient-derived Organoids as a Promising Tool for Multimodal Management of Sarcomas. Cancers (Basel). 2023;15(17).
7. Broutier L, Mastrogiovanni G, Verstegen MM, Francies HE, Gavarró LM, Bradshaw CR, et al. Human primary liver cancer-derived organoid cultures for disease modeling and drug screening. Nat Med. 2017;23(12):1424–35.

8. Driehuis E, Kretzschmar K, Clevers H. Establishment of patient-derived cancer organoids for drug-screening applications. Nat Protoc. 2020;15(10):3380–409.
9. Guillen KP, Fujita M, Butterfield AJ, Scherer SD, Bailey MH, Chu Z, et al. A human breast cancer-derived xenograft and organoid platform for drug discovery and precision oncology. Nat Cancer. 2022;3(2):232–50.
10. Yan HHN, Siu HC, Law S, Ho SL, Yue SSK, Tsui WY, et al. A Comprehensive Human gastric Cancer Organoid Biobank captures Tumor Subtype Heterogeneity and enables therapeutic screening. Cell Stem Cell. 2018;23(6):882–e9711.
11. Weng W, Meng T, Zhao Q, Shen Y, Fu G, Shi J, et al. Antibody-exatecan conjugates with a Novel Self-immolative Moiety overcome resistance in Colon and Lung Cancer. Cancer Discov. 2023;13(4):950–73.
12. Su L, Chen Y, Huang C, Wu S, Wang X, Zhao X, et al. Targeting src reactivates pyroptosis to reverse chemoresistance in lung and pancreatic cancer models. Sci Transl Med. 2023;15(678):eabl7895.
13. Tong X, Patel AS, Kim E, Li H, Chen Y, Li S, et al. Adeno-to-squamous transition drives resistance to KRAS inhibition in LKB1 mutant lung cancer. Cancer Cell. 2024;42(3):413–e287.
14. Wang HM, Zhang CY, Peng KC, Chen ZX, Su JW, Li YF, et al. Using patient-derived organoids to predict locally advanced or metastatic lung cancer tumor response: a real-world study. Cell Rep Med. 2023;4(2):100911.
15. Kim M, Mun H, Sung CO, Cho EJ, Jeon HJ, Chun SM, et al. Patient-derived lung cancer organoids as in vitro cancer models for therapeutic screening. Nat Commun. 2019;10(1):3991.
16. Hu Y, Sui X, Song F, Li Y, Li K, Chen Z, et al. Lung cancer organoids analyzed on microwell arrays predict drug responses of patients within a week. Nat Commun. 2021;12(1):2581.
17. Vlachogiannis G, Hedayat S, Vatsiou A, Jamin Y, Fernández-Mateos J, Khan K, et al. Patient-derived organoids model treatment response of metastatic gastrointestinal cancers. Science. 2018;359(6378):920–6.
18. Neal JT, Li X, Zhu J, Giangarra V, Grzeskowiak CL, Ju J, et al. Organoid modeling of the Tumor Immune Microenvironment. Cell. 2018;175(7):1972–e8816.
19. Dao V, Yuki K, Lo YH, Nakano M, Kuo CJ. Immune organoids: from tumor modeling to precision oncology. Trends Cancer. 2022;8(10):870–80.
20. Zhang J, Tavakoli H, Ma L, Li X, Han L, Li X. Immunotherapy discovery on tumor organoid-on-a-chip platforms that recapitulate the tumor microenvironment. Adv Drug Deliv Rev. 2022;187:114365.
21. Meng F, Shen C, Yang L, Ni C, Huang J, Lin K, et al. Mechanical stretching boosts expansion and regeneration of intestinal organoids through fueling stem cell self-renewal. Cell Regen. 2022;11(1):39.
22. Kobayashi H, Gieniec KA, Lannagan TRM, Wang T, Asai N, Mizutani Y, et al. The origin and contribution of Cancer-Associated fibroblasts in colorectal carcinogenesis. Gastroenterology. 2022;162(3):890–906.
23. Tuveson D, Clevers H. Cancer modeling meets human organoid technology. Science. 2019;364(6444):952–5.
24. Ugurlu B, Karaoz E. Comparison of similar cells: mesenchymal stromal cells and fibroblasts. Acta Histochem. 2020;122(8):151634.
25. Mishra PJ, Mishra PJ, Humeniuk R, Medina DJ, Alexe G, Mesirov JP, et al. Carcinoma-associated fibroblast-like differentiation of human mesenchymal stem cells. Cancer Res. 2008;68(11):4331–9.
26. Guo L, Cui C, Zhang K, Wang J, Wang Y, Lu Y, et al. Kindlin-2 links mechano-environment to proline synthesis and tumor growth. Nat Commun. 2019;10(1):845.
27. Sossey-Alaoui K, Pluskota E, Bialkowska K, Szpak D, Parker Y, Morrison CD, et al. Kindlin-2 regulates the growth of breast Cancer tumors by activating CSF-1-Mediated macrophage infiltration. Cancer Res. 2017;77(18):5129–41.
28. Theodosiou M, Widmaier M, Böttcher RT, Rognoni E, Veelders M, Bharadwaj M, et al. Kindlin-2 cooperates with talin to activate integrins and induces cell spreading by directly binding paxillin. Elife. 2016;5:e10130.
29. Zhang P, Wang J, Luo W, Yuan J, Cui C, Guo L, et al. Kindlin-2 acts as a key mediator of lung fibroblast activation and pulmonary fibrosis progression. Am J Respir Cell Mol Biol. 2021;65(1):54–69.
30. Yin SY, Liu YJ, Li JP, Liu J. Overexpression of FERM Domain Containing Kindlin 2 (FERMT2) in fibroblasts correlates with EMT and immunosuppression in gastric Cancer. Int J Genomics. 2024;2024:4123737.
31. He Y, Esser P, Schacht V, Bruckner-Tuderman L, Has C. Role of kindlin-2 in fibroblast functions: implications for wound healing. J Invest Dermatol. 2011;131(1):245–56.
32. Moslem M, Eggenschwiler R, Wichmann C, Buhmann R, Cantz T, Henschler R. Kindlin-2 modulates the survival, differentiation, and Migration of Induced Pluripotent cell-derived mesenchymal stromal cells. Stem Cells Int. 2017;2017:7316354.
33. Wang J, Sui Z, Huang W, Yu Z, Guo L. Biomimetic hydrogels with mesoscale collagen architecture for patient-derived tumor organoids culture. Bioactive Mater. 2024;38:384–98.
34. Chen S, Zhou Y, Chen Y, Gu J. Fastp: an ultra-fast all-in-one FASTQ preprocessor. Bioinformatics. 2018;34(17):i884–90.
35. Li H, Durbin R. Fast and accurate short read alignment with Burrows-Wheeler transform. Bioinformatics. 2009;25(14):1754–60.
36. Cibulskis K, Lawrence MS, Carter SL, Sivachenko A, Jaffe D, Sougnez C, et al. Sensitive detection of somatic point mutations in impure and heterogeneous cancer samples. Nat Biotechnol. 2013;31(3):213–9.
37. Wang K, Li M, Hakonarson H. ANNOVAR: functional annotation of genetic variants from high-throughput sequencing data. Nucleic Acids Res. 2010;38(16):e164.
38. Talevich E, Shain AH, Botton T, Bastian BC, CNVkit. Genome-wide Copy Number Detection and visualization from targeted DNA sequencing. PLoS Comput Biol. 2016;12(4):e1004873.
39. Guo L, Zhou Y, Wang S, Wu Y. Epigenetic changes of mesenchymal stem cells in three-dimensional (3D) spheroids. J Cell Mol Med. 2014;18(10):2009–19.
40. Wang S, Guo L, Ge J, Yu L, Cai T, Tian R, et al. Excess integrins cause lung entrapment of mesenchymal stem cells. Stem Cells. 2015;33(11):3315–26.
41. Hoang DM, Pham PT, Bach TQ, Ngo ATL, Nguyen QT, Phan TTK, et al. Stem cell-based therapy for human diseases. Signal Transduct Target Ther. 2022;7(1):272.
42. Zhou T, Yuan Z, Weng J, Pei D, Du X, He C, et al. Challenges and advances in clinical applications of mesenchymal stromal cells. J Hematol Oncol. 2021;14(1):24.
43. Lin Z, Wu Y, Xu Y, Li G, Li Z, Liu T. Mesenchymal stem cell-derived exosomes in cancer therapy resistance: recent advances and therapeutic potential. Mol Cancer. 2022;21(1):179.
44. Zou Z, Lin Z, Wu C, Tan J, Zhang J, Peng Y, et al. Micro-engineered Organoid-on-a-Chip based on mesenchymal stromal cells to predict immunotherapy responses of HCC patients. Adv Sci (Weinh). 2023;10(27):e2302640.
45. Nuciforo S, Fofana I, Matter MS, Blumer T, Calabrese D, Boldanova T, et al. Organoid models of Human Liver cancers derived from Tumor needle biopsies. Cell Rep. 2018;24(5):1363–76.
46. Lee D, Kim Y, Chung C. Scientific validation and clinical application of Lung Cancer Organoids. Cells. 2021;10(11).
47. Servant R, Garioni M, Vlajnic T, Blind M, Pueschel H, Müller DC, et al. Prostate cancer patient-derived organoids: detailed outcome from a prospective cohort of 81 clinical specimens. J Pathol. 2021;254(5):543–55.
48. Evans RA, Tian YC, Steadman R, Phillips AO. TGF-beta1-mediated fibroblast-myofibroblast terminal differentiation-the role of smad proteins. Exp Cell Res. 2003;282(2):90–100.
49. Paunescu V, Bojin FM, Tatu CA, Gavriliuc OI, Rosca A, Gruia AT, et al. Tumour-associated fibroblasts and mesenchymal stem cells: more similarities than differences. J Cell Mol Med. 2011;15(3):635–46.
50. Saxena N, Chakraborty S, Dutta S, Bhardwaj G, Karnik N, Shetty O et al. Stiffness-dependent MSC homing and differentiation into CAFs - implications for breast cancer invasion. J Cell Sci. 2024;137(1).
51. Kalluri R. The biology and function of fibroblasts in cancer. Nat Rev Cancer. 2016;16(9):582–98.
52. Li H, Deng Y, Sun K, Yang H, Liu J, Wang M, et al. Structural basis of kindlin-mediated integrin recognition and activation. Proc Natl Acad Sci U S A. 2017;114(35):9349–54.
53. Tu Y, Wu S, Shi X, Chen K, Wu C. Migfilin and Mig-2 link focal adhesions to filamin and the actin cytoskeleton and function in cell shape modulation. Cell. 2003;113(1):37–47.

Publisher's note